



Simulations of electron capture and low-mass iron core supernovae

B. Müller^{1,2}, S. Wanajo^{3,4}, H.-Th. Janka⁵, A. Heger², D. Gay¹, and S.A. Sim¹

¹ Astrophysics Research Centre, School of Mathematics and Physics, Queens University Belfast, Belfast, BT7 1NN, United Kingdom, e-mail: b.mueller@qub.ac.uk

² Monash Centre for Astrophysics, School of Physics and Astronomy, Monash University, VIC 3800, Australia

³ Department of Engineering and Applied Sciences, Sophia University, Chiyoda-ku, Tokyo 102-8554, Japan

⁴ iTHES Research Group, RIKEN, Wako, Saitama 351-0198, Japan

⁵ Max-Planck-Institut für Astrophysik, Karl-Schwarzschild-Str. 1, 85748 Garching, Germany

Abstract. The evolutionary pathways of core-collapse supernova progenitors at the low-mass end of the spectrum are beset with major uncertainties. In recent years, a variety of evolutionary channels has been discovered in addition to the classical electron capture supernova channel of super-AGB stars. The few available progenitor models at the low-mass end have been studied with great success in supernova simulations as the peculiar density structure makes for robust neutrino-driven explosions in this mass range. Detailed nucleosynthesis calculations have been conducted both for models of electron capture supernovae and low-mass iron core supernovae and revealed an interesting production of the lighter trans-iron elements (such as Zn, Sr, Y, Zr) as well as rare isotopes like ⁴⁸Ca and ⁶⁰Fe. We stress the need to explore the low-mass end of the supernova spectrum further and link various observables to understand the diversity of explosions in this regime.

1. Introduction

The region just above the minimum mass for core-collapse supernova (SN) explosions is of particular interest for supernova theory for several reasons. Due to the steepness of the initial mass function, roughly 20% of core-collapse events originate from progenitors within $2M_{\odot}$ of this minimum mass on the zero-age main sequence.

From the point of view of stellar evolution, the lower end of the mass range for core-collapse SNe is remarkably different from generic high-mass progenitors. Contrary to higher masses, degeneracy and off-centre igni-

tion play a major role during the evolution beyond carbon burning, which lead to structural peculiarities of the progenitors. The classical “electron capture supernova” (ECSN) channel for super-AGB progenitors (SAGB) best exemplifies these peculiarities (Nomoto 1984, 1987). Here collapse is triggered by electron captures on ²⁰Ne and ²⁴Mg in a degenerate O-Ne-Mg core, which is separated merely by a tiny C/O layer from the H envelope as the He shell has been eliminated by dredge-up. While the width of the classical ECSN channel is beset with uncertainties such as our incomplete understanding of O ignition and flame propagation (Timmes & Woosley 1992; Timmes

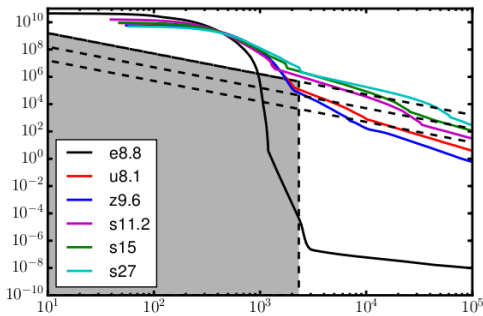


Fig. 1. Density profiles of an ECSN progenitor (e8.8, Nomoto 1984), low-mass iron core progenitors with $8.1M_{\odot}$ (u8.1, $Z = 10^{-4}Z_{\odot}$) and $9.6M_{\odot}$ (z9.6, $Z = 0$), and more massive progenitors with $11.2M_{\odot}$, $27M_{\odot}$ (s11.2 and s27, Woosley et al. 2002) and $15M_{\odot}$ (Woosley & Weaver 1995). The approximate accretion rate is indicated by slanted dashed lines ($0.05M_{\odot} \text{ s}^{-1}$, $0.005M_{\odot} \text{ s}^{-1}$, and $5 \times 10^{-4}M_{\odot} \text{ s}^{-1}$ from the top). The vertical dashed line roughly indicates an infall time of 0.5 s. ECSN-like explosions with fast shock expansion and without significant accretion after shock revival are expected in the grey-shaded region (see Müller 2016 for details). Note that the low-mass iron core progenitors only marginally fall into this regime and that the transition from the “ECSN-like” regime to normal supernovae is not abrupt in reality.

et al. 1994; Jones et al. 2016), studies of the AGB-SN mass transition in recent years (Jones et al. 2013, 2014; Doherty et al. 2015, 2017; Woosley & Heger 2015) have unearthed a variety of pathways towards collapse that lead to a similar – though sometimes less extreme – progenitor structure characterised by a strongly degenerate core with a very steep density gradient into the surrounding tenuous shells.

While the intricacies of stellar evolution at the AGB-SN mass transition still present a challenge, this mass range has been a particularly fruitful target for first-principle supernova simulations for the last decade since the first modern ECSN explosion model of Kitaura et al. (2006). Contrary to more massive progenitors, the explosion mechanism close to this transition is understood to the degree that neutrino-driven explosions are readily obtained in self-consistent simulations in 1D (Kitaura et al. 2006; Fischer et al. 2010;

Hüdepohl et al. 2009; Melson et al. 2015; Radice et al. 2017), 2D (Wanajo et al. 2011; Müller et al. 2012; Janka et al. 2012; Radice et al. 2017), and 3D (Melson et al. 2015).

2. Explosion dynamics of electron capture and low-mass iron core supernovae

The critical structural feature behind the robustness of neutrino-driven shock revival close to the AGB-SN mass transition is the steep density gradient outside the core (Fig. 1). This results in a rapid drop of the mass accretion rate \dot{M} onto the proto-neutron star (of mass M) soon after bounce, which is related to the initial density ρ of infalling shells from radius r as $\dot{M} \approx 8\pi\rho\sqrt{Gmr^3}/3$. Consequently, the stagnation radius of the shock increases due to the lower pre-shock ram pressure, conditions become favourable to neutrino-driven runaway shock expansion in low-mass SN progenitors early on.

As \dot{M} plummets rapidly, these explosions do not exhibit an extended phase of concurrent accretion and mass ejection after shock revival, which can last for seconds in more massive progenitors (Müller 2015; Bruenn et al. 2016; Müller et al. 2017). Without such a cycle of accretion and mass ejection, the explosion energy is essentially set by the mass in the gain region around the onset of shock revival. Once the ejected matter is unbound by neutrino heating, the residual net contribution to the explosion energy is provided by the recombination of nucleons into heavy nuclei and α -particles (Janka et al. 2008). The ejection of $\sim 0.01M_{\odot}$ results in a small explosion energy of $\sim (0.5 \dots 1) \times 10^{50}$ erg with a small additional contribution from the neutrino-driven wind on longer time-scales. The explosion dynamics allows only for the production of a small amount of radioactive ^{56}Ni of the order of $10^{-3}M_{\odot}$.

Although shock revival is found even in 1D models of progenitors close to the AGB-SN transition, multi-D effects are not negligible for the explosion dynamics, especially for models with less extreme density profiles. While multi-D effects only boost the explosion energy by $\sim 10\%$ in models of the classical ECSN

channel, they do enhance the explosion energy by a factor of several for low-mass iron core progenitors with more substantial C/O and He shells (Melson et al. 2015; Radice et al. 2017). Nevertheless, rapid shock revival and the absence of an extended phase of concurrent accretion and mass ejection motivate classifying such explosions as “ECSN-like” as opposed to SNe from more massive progenitors.

3. Nucleosynthesis in the neutrino-processed ejecta

The peculiar explosion dynamics and progenitor structure close to the AGB-SN transition have interesting implications for the nucleosynthesis in this range. Since the ejected mass from the tenuous shells (He, C, O) between the core and the hydrogen envelope is small, primary and secondary hydrostatic and explosive burning processes in these shells do not contribute significantly in terms of production factors. Instead, the yields for the least massive supernova progenitors are *dominated* by the neutrino-heated material from the gain region, whose composition, entropy s , and electron fraction Y_e are *completely reset* into an equilibrium determined by neutrino and electron/positron capture reactions $p(\bar{\nu}_e, e^+)n$, $n(\nu_e, e^-)p$, $p(e^-, \nu_e)n$, and $n(e^+, \bar{\nu}_e)p$ in the vicinity of the proto-neutron star before it is ejected. The progenitor’s composition and metallicity therefore do not affect the yields directly. They merely have an indirect effect via the progenitor structure, e.g., through the metallicity-dependent location of the AGB-SN transition (Ibeling & Heger 2013) and the width of the ECSN channel (Poelarends et al. 2008).

These “innermost” neutrino-driven ejecta are indeed relevant for the nucleosynthesis contributions of core-collapse SNe and the distribution of radionuclides in SN remnants across a wider mass range of progenitors (Pruet et al. 2006; Wongwathanarat et al. 2016; Wanajo et al. 2017). ECSNe, however, represent the first case for which the complete nucleosynthesis in the innermost ejecta could be studied in detail based on self-consistent multi-D explosion models of the early explo-

sion phase (Wanajo et al. 2011, 2013a,b) and 1D models of the subsequent neutrino-driven wind phase (Wu et al. 2014; Pllumbi et al. 2015). The key difficulty here lies in accurately capturing the evolution of Y_e in the innermost ejecta, which requires rigorous neutrino transport (including even the effects of neutrino flavour conversion near the proto-neutron star) to correctly model differences in the electron neutrino and antineutrino emission in contrast to simulations relying on pistons and thermal bombs (e.g., Rauscher et al. 2002; Limongi & Chieffi 2003; Tominaga et al. 2007; Heger & Woosley 2010; Nomoto et al. 2013; Chieffi & Limongi 2013). Second, the multi-D explosion dynamics is relevant as it determines the freeze-out of Y_e at a radius where $r \sim \langle E_\nu \rangle / (m_N \dot{q}_\nu v_r)$ in terms of the nucleon mass m_N , the mass specific heating rate \dot{q}_ν , the ejection velocity v_r and the averaged mean energy $\langle E_\nu \rangle$ of ν_e and $\bar{\nu}_e$ (Qian & Woosley 1996; Müller 2016). Finally, simulations need to be evolved sufficiently far to capture the bulk of the neutrino-heated ejecta and safely demarcate the actual ejecta from fallback material, which is an impediment for multi-D explosion models of more massive stars (Wanajo et al. 2017) and has so far limited us to axisymmetric (2D) models as input for nucleosynthesis calculations. Nevertheless, a comparison of essentially complete yields for ECSN-like explosions and the early neutrino-heated ejecta in SNe from more massive progenitors is already possible and reveals pronounced differences.

4. Neutrino-heated ejecta in low-mass supernovae

The key to these differences lies in the development of overturn driven by the Rayleigh-Taylor instability in the wake of the rapidly expanding shock between deeper layers of high-entropy neutrino-driven ejecta and colder ejecta shocked at early times. Due to high ejection velocities, Y_e in the rising bubbles freezes out closer to the proto-neutron star at $Y_e \approx 0.4$ (Fig. 2). Entropies are modest ($\sim 15k_b/\text{nucleon}$) in the most neutron-rich ejecta and higher in the more slowly expanding ejecta that have been exposed to neutron

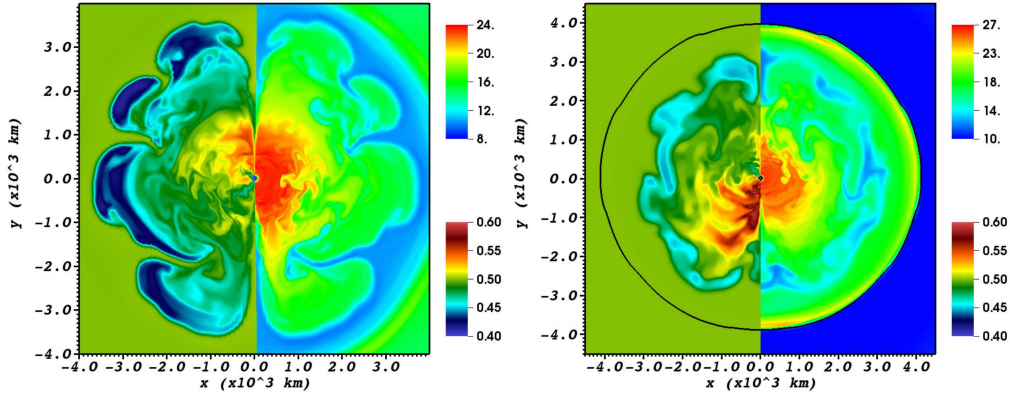


Fig. 2. Electron fraction Y_e (left half of panels) and entropy s (right half of panels) in 2D simulations of an ECSN (left, 266 ms after bounce, progenitor e8.8) and in a low-mass iron core supernova (right, 317 ms after bounce, progenitor z9.6). Both show similar neutron-rich Rayleigh-Taylor plumes that develop shortly after shock revival.

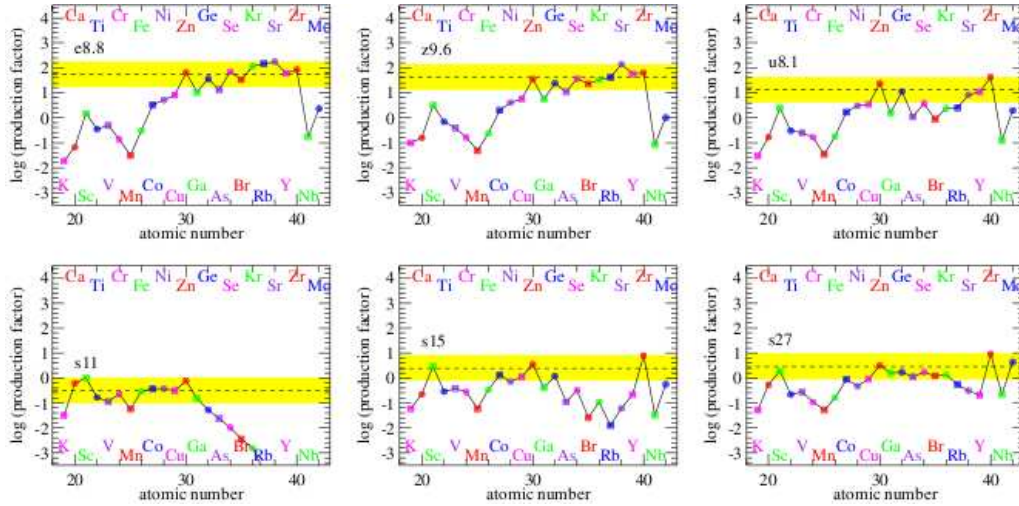


Fig. 3. Elemental production factors for the ECSN model e8.8 and the low-mass iron core models z9.6 and u8.1 (top row) compared to the production factors for the more massive progenitor s11.2, s15, and s27 (bottom row), taken from Wanajo et al. (2017). The production factors are defined as the ratio of mass fraction of an element in the ejecta and the corresponding solar value (Lodders 2003). The yellow bands denote a range of 1 dex in production factor below the maximum value for each progenitor.

heating longer. Wanajo et al. (2011) showed that for ECSNe the resulting nucleosynthesis is a combination of freeze-out from α -deficient QSE for $Y_e < 0.43$ and α -rich QSE for $0.43 < Y_e < 0.49$ with relatively uniform production factors between Zn and Zr (Fig. 3, top

left). There is also a significant production of the neutron-rich radionuclides ^{48}Ca (Wanajo et al. 2013a) and ^{60}Fe (Wanajo et al. 2013b). Subsequent work by Wanajo et al. (2017) indicates that the explosion dynamics of low-mass iron core progenitors is sufficiently extreme to

attain the same or at least similar neutron-rich nucleosynthesis in low-mass iron-core progenitors with $9.6M_{\odot}$ (zero metallicity) and $8.1M_{\odot}$ (metallicity $Z = 10^{-4}Z_{\odot}$) as shown in Fig. 3 (top row, middle and right).

Slower shock propagation, by contrast, impedes the ejection of neutron-rich plumes in more massive progenitors with slower shock propagation, which leads to characteristically different yields from proton-rich ejecta (bottom row of Fig. 3). Somewhat similar yield patterns in the atomic mass range of $A = 30 \dots 40$ may, however, also occur for more massive progenitors, as for example in the $27M_{\odot}$ model of Wanajo et al. (2017), where this results from the ejection of some neutron-rich material in a rather early explosion and a weak νp -process in the proto-rich ejecta.

At present, the comparison of nucleosynthesis yields in ECSN-like explosions and SNe from more massive progenitors remains beset with many imponderables, including the impact of neutrino rate uncertainties and neutrino flavour conversion (investigated in the context of 1D explosion models by Wu et al. 2014 and Pillumbi et al. 2015), 3D effects on plume ejection (Müller 2016), the LESA instability (Tamborra et al. 2014) in 3D, resolution effects and our incomplete understanding of the explosions of more massive progenitors.

Nonetheless, self-consistent SN models already suggest that ECSN-like explosions play a significant role in a comprehensive picture of chemical evolution, e.g. as a source that produces $N = 50$ nuclei (Sr, Y, Zr) without the heavy r-process elements as required by observed abundance trends (Travaglio et al. 2004; Wanajo & Ishimaru 2006; Qian & Wasserburg 2008; Hansen et al. 2013), or as a source of ^{48}Ca whose origin remains poorly understood.

5. Outlook

With the emerging links between stellar evolution, SN modelling, and chemogalactic evolution in the case of ECSNe and low-mass iron core supernovae, there is an opportunity to better constrain the considerable uncertainties that beset the evolution of the least massive core-collapse SNe progenitors. The mod-

els of recent years only constitute the first step in this undertaking. With respect to SN simulations, some of the salient uncertainties, such as the lack of 3D first-principle modes, have already been mentioned. Moreover, SN simulations need to scan the low-mass end of the spectrum more thoroughly given the multiplicity of subtly different stellar evolution channels in a small mass window.

In addition to encouraging progress in confronting models of ECSN-like explosions with nucleosynthesis constraints, it remains imperative to better understand the nature of the diverse low-energy transients that are *prima facie* suggestive of ECSN-like explosion dynamics with low explosion energies and small nickel masses. Noteworthy results on the light curve of SN 1054 (the Crab supernova) and various Type II_n-P SNe have been obtained recently (Tominaga et al. 2013; Moriya et al. 2014) to strengthen the suggested link between ECSNe and these events (e.g., Smith 2013). Progenitor detections (or upper limits on progenitor brightness in lieu of a positive detection) are also helping to match low-energy transients to the various SN channels close to the AGB-SN mass transition (SN 2005cs: Eldridge et al. 2007s, SN 2008S: Botticella et al. 2009). Distinguishing these channels by means of observations remains a challenge, however, and a definitive “smoking gun” for the classical ECSN channel of SAGB stars is still missing. A better connection of stellar evolution and explosion models to the signatures of the photospheric and nebular phase (see A. Jerkstrand, these proceedings) is still needed to accomplish this.

Acknowledgements. We acknowledge support by ARC grants DE150101145 (BM) and FT120100363 (AH), STFC grant ST/P000312/1 (BM), by the RIKEN iTHES Project, the JSPS Grants-in-Aid for Scientific Research (26400232, 26400237) (SW), the Deutsche Forschungsgemeinschaft (EXC 153), by the ERC grant ERC-AdG No. 341157-COCO2CASA (TJ), and NSF Grant No. PHY-1430152 through JINA-CEE (AH, BM). Supercomputer time at the National Computational Infrastructure (NCI), the Pawsey Supercomputing Centre, the Max Planck Computing and Data Facility, the Minnesota Supercomputing Institute,

and the Dirac Data Centric system (Durham) is acknowledged.

References

- Botticella, M. T., Pastorello, A., Smartt, S. J., et al. 2009, *MNRAS*, 398, 1041
- Bruenn, S. W., Lentz, E. J., Hix, W. R., et al. 2016, *ApJ*, 818, 123
- Chieffi, A. & Limongi, M. 2013, *ApJ*, 764, 21
- Doherty, C. L., et al. 2015, *MNRAS*, 446, 2599
- Doherty, C. L., et al. 2017, *ArXiv e-prints* [arXiv:1703.06895]
- Eldridge, J. J., Mattila, S., & Smartt, S. J. 2007, *MNRAS*, 376, L52
- Fischer, T., et al. 2010, *A&A*, 517, A80
- Hansen, C. J., Bergemann, M., Cescutti, G., et al. 2013, *A&A*, 551, A57
- Heger, A. & Woosley, S. E. 2010, *ApJ*, 724, 341
- Hüdepohl, L., et al. 2009, *Phys. Rev. Lett.*
- Ibeling, D. & Heger, A. 2013, *ApJ*, 765, L43
- Janka, H.-T., et al. 2008, *A&A*, 485, 199
- Janka, H.-T., Hanke, F., Hüdepohl, L., et al. 2012, *Progress of Theoretical and Experimental Physics*, 2012, 010000
- Jones, S., Hirschi, R., Nomoto, K., et al. 2013, *ApJ*, 772, 150
- Jones, S., Hirschi, R., & Nomoto, K. 2014, *ApJ*, 797, 83
- Jones, S., Roepke, F. K., Pakmor, R., et al. 2016, *A&A*, 593, A72
- Kitaura, F. S., Janka, H.-T., & Hillebrandt, W. 2006, *A&A*, 450, 345
- Limongi, M. & Chieffi, A. 2003, *ApJ*, 592, 404
- Lodders, K. 2003, *ApJ*, 591, 1220
- Melson, T., Janka, H.-T., & Marek, A. 2015, *ApJ*, 801, L24
- Moriya, T. J., Tominaga, N., Langer, N., et al. 2014, *A&A*, 569, A57
- Müller, B. 2015, *MNRAS*, 453, 287
- Müller, B. 2016, *PASA*, 33, e048
- Müller, B., Janka, H.-T., & Heger, A. 2012, *ApJ*, 761, 72
- Müller, B., Melson, T., Heger, A., & Janka, H.-T. 2017, *ArXiv e-prints* [arXiv:1705.00620]
- Nomoto, K. 1984, *ApJ*, 277, 791
- Nomoto, K. 1987, *ApJ*, 322, 206
- Nomoto, K., Kobayashi, C., & Tominaga, N. 2013, *ARA&A*, 51, 457
- Pllumbi, E., et al. 2015, *ApJ*, 808, 188
- Poelarends, A. J. T., et al. 2008, *ApJ*, 675, 614
- Pruet, J., et al. 2006, *ApJ*, 644, 1028
- Qian, Y. & Woosley, S. E. 1996, *ApJ*, 471, 331
- Qian, Y.-Z. & Wasserburg, G. J. 2008, *ApJ*, 687, 272
- Radice, D., et al. 2017, *ArXiv e-prints* [arXiv:1702.03927]
- Rauscher, T., et al. 2002, *ApJ*, 576, 323
- Smith, N. 2013, *MNRAS*, 434, 102
- Tamborra, I., Hanke, F., Janka, H.-T., et al. 2014, *ApJ*, 792, 96
- Timmes, F. X. & Woosley, S. E. 1992, *ApJ*, 396, 649
- Timmes, F. X., Woosley, S. E., & Taam, R. E. 1994, *ApJ*, 420, 348
- Tominaga, N., Blinnikov, S. I., & Nomoto, K. 2013, *ApJ*, 771, L12
- Travaglio, C., Gallino, R., Arnone, E., et al. 2004, *ApJ*, 601, 864
- Tominaga, N., Umeda, H., & Nomoto, K. 2007, *ApJ*, 660, 516
- Wanajo, S. & Ishimaru, Y. 2006, *Nuclear Physics A*, 777, 676
- Wanajo, S., Janka, H.-T., & Müller, B. 2011, *ApJ*, 726, L15
- Wanajo, S., Janka, H.-T., & Müller, B. 2013a, *ApJ*, 767, L26
- Wanajo, S., Janka, H.-T., & Müller, B. 2013b, *ApJ*, 774, L6
- Wanajo, S., Müller, B., Janka, H.-T., & Heger, A. 2017, *ArXiv e-prints* [arXiv:1701.06786]
- Wongwathanarat, A., et al. 2016, *ArXiv e-prints* [arXiv:1610.05643]
- Woosley, S. E. & Heger, A. 2015, *ApJ*, 810, 34
- Woosley, S. E., Heger, A., & Weaver, T. A. 2002, *Rev. Mod. Phys.*, 74, 1015
- Woosley S. E., Weaver T. A. 1995, *ApJS*, 101, 181
- Wu, M.-R., et al. 2014, *Phys. Rev. D*, 89, 061303